MAK HILL Publications
ACE Journal of Advance Research In Physical Sciences
Research Article
doi: acejarcs.2023.10.17

OPEN ACCESS

Key Words
Barium oxide, simple chemical method, solar cell, photodetector

Corresponding Author
Nazar Abdulmahdi Jabir Al Wassiti, Department of Physics, Faculty of Science, Mustansiriyah University, Baghdad, Iraq

Received: 15 January 2023
Accepted: 20 January 2023
Published: 25 January 2023

Citation: Nazar Abdulmahdi Jabir Al Wassiti, Wedian K. Abad and Ahmed N. Abd, 2023. Synthesis of Barium Oxide Nanoparticles by Simple Chemical Method and its Applications as a Solar Cell and Photodetector. ACE J. Adv. Res. Phys. Sci., XX: 00-00, doi:

Synthesis of Barium Oxide Nanoparticles by Simple Chemical Method and its Applications as a Solar Cell and Photodetector

[1]Nazar Abdulmahdi Jabir Al Wassiti, [2]Wedian K. Abad and [1]Ahmed N. Abd

[1]*Department of Physics, Faculty of Science, Mustansiriyah University, Baghdad, Iraq*
[2]*Applied Physics Branch, Department of Applied Science, University of Technology, Iraq*

ABSTRACT
Barium oxide (BaONPs) is synthesized using a straightforward chemical process. Through X-ray diffraction, the creation of cubic-structure BaO nanoparticles was verified (XRD). BaO predicted crystallite sizes from X-ray diffraction (XRD) data were 66.23 nm. Utilizing an AFM with a scanning electron microscope to investigate morphology BaO computed band gap energy was 4.35 eV. The presence of the (BaO) stretching vibration mode is indicated by the emergence of the transmission peak at 670 cm^{-1} in the FTIR spectrum. It was found from current-voltage measurements under illumination that the performance of the solar cell is good where the solar cell achieved efficiency (η = 0.48%). Also the Photodetector has been successfully fabricated, where the results indicate that it can be used for detection.

INTRODUCTION

Sustainable energy sources are a defining feature of the contemporary global industrialization age. For countries to benefit from the industrial revolution, they must have access to inexpensive, sustainable and clean energy. Solar energy is one potential energy source that is safe, environmentally friendly and reasonably priced[1-3]. Regarding solar cells, there have been changes in cost, toxicity and efficiency. A high efficiency but expensive inorganic silicon wafer was utilized in the first generation of solar cells. The second generation uses highly efficient, toxic and environmentally dangerous inorganic thin films (CIGS, CdTe). The third-generation solar cells are organic thin films, which are easy to produce at low cost and have a better efficiency[4-6]. Due to their incredible qualities and wide variety of uses, nanomaterials are being prepared by the majority of researchers. These are particularly utilized in electrochemical and photovoltaic cell applications for energy. Improvements in nanomaterial manufacturing have advanced significantly over the past several years because to the distinct electrical, optical, mechanical, magnetic and chemical characteristics of nanomaterials, which differ greatly from those of bulk materials. Whereas a number of scientific sectors have paid close attention to metal oxide nanoparticles in particular[7-9]. BaO is a group II-VI semiconductor nanomaterial with a direct band gap of 4.4 eV that is employed in a variety of applications, including as self-cleaning, electrical energy production, sensors and actuators, the pharmaceutical sector and catalysts. In order to create nanomaterials of diverse sizes and shapes, a number of BaO Nanoparticles (BaO-NPs) production techniques, including sol-gel, chemical, hydrothermal, thermal decomposition, sonochemical, microwave irradiation and fast precipitation, have been developed to date[10-17]. The purpose of this article was to fabricate heterojunction for use in solar cells and detector applications, examine the characteristics of BaO NPs using XRD, SEM, AFM, UV and FTIR and fabricate them using a straightforward chemical technique.

MATERIALS AND METHODS

Merck supplied the precursor substances sodium hydroxide (NaOH) and barium nitrate $(BaNO_3)_2$. With the aid of a magnetic stirrer, 0.1 M (2.61 g) of barium nitrate $(BaNO_3)_2$ was entirely dissolved in 100 mL of deionized water (H_2O) in about 30 min. Similar to this, 100 mL of deionized water (H_2O) was mixed with 0.5 M (2 g) of sodium hydroxide pellets until the NaOH entirely dissolved using a magnetic stirrer for around 30 min. Following that, as indicated in Fig. 1, the sodium hydroxide (NaOH) solution was added dropwise (3 mL) to the $(BaNO_3)_2$ solution while it was continuously stirred for 1 h at 70°C. The reaction mixture transforms into a white precipitate throughout this procedure. The precipitate was cleaned four times with distilled water before being centrifuged to get rid of any remaining native contaminants.

RESULTS AND DISSUASIONS

Figure 2 shows the X-ray diffraction of barium oxide nanoparticles that prepared by simple chemical method and deposited by drop casting on glasses substrate. The diffraction peaks are observed at values 21.7°, 24.51°, 38.72°, 44.00°, 59.21° and 74.82° for BaO corresponding to: 200, 100, 111, 101, 111, 103, 114 and 223, respectively. The average grain size of BaO nanoparticles synthetized by chemical synthesis was determined using Debye-Scherrer equation was 66.23 nm[9,18,19].

BaO nanostructure's surface morphology was examined using scanning electron microscopy. According to the BaO SEM picture (Fig. 3), the material is made up of evenly scattered, porous, some

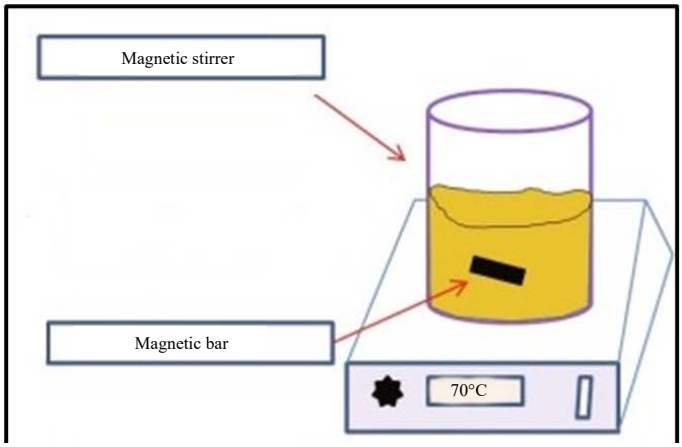

Fig. 1: Simple chemical method for prepared BaO Nps

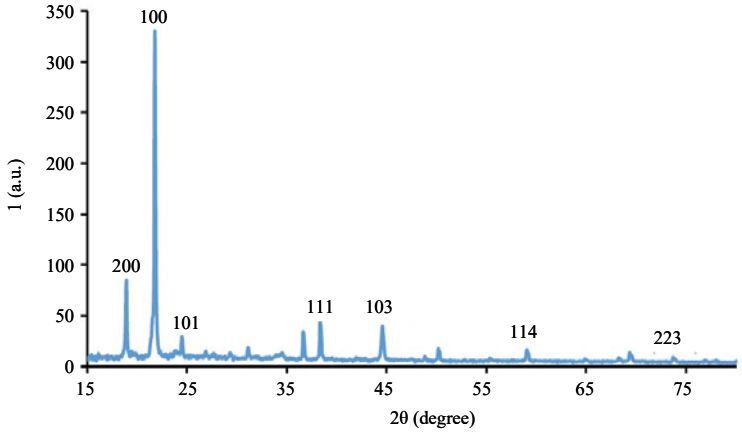

Fig. 2: XRD of BaO thin film

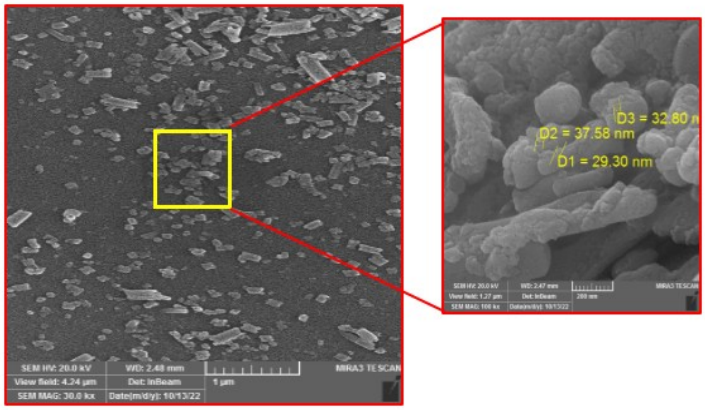

Fig. 3: Images SEM of BaO thin film

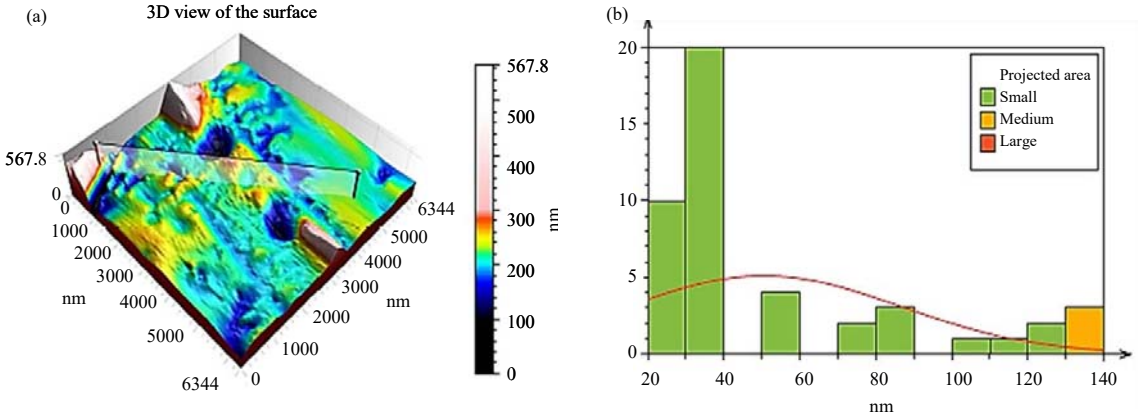

Fig. 4: AFM of BaO thin film

agglomerated and flower-like nanoparticles with an average diameter of 33.22 nm. As shown in Fig. 4, BaO nanoparticles were studied using atomic force microscopy (AFM), which revealed that they are round or oval in form, with an average particle size of 56.7 nm, a root mean square of 56.59 nm and a roughness of 43.07 nm.

A UV-visible (UV-Vis) spectrophotometer is often used to study the optical characteristics of BaO-NPs. The transmittance spectra of BaO colloidal are displayed in Fig. 5a in the 200-1100 nm range. After the wavelength >300, the transmittance of the thin films is high, between 60 and 79% in the visible range and IR, which makes them ideal for

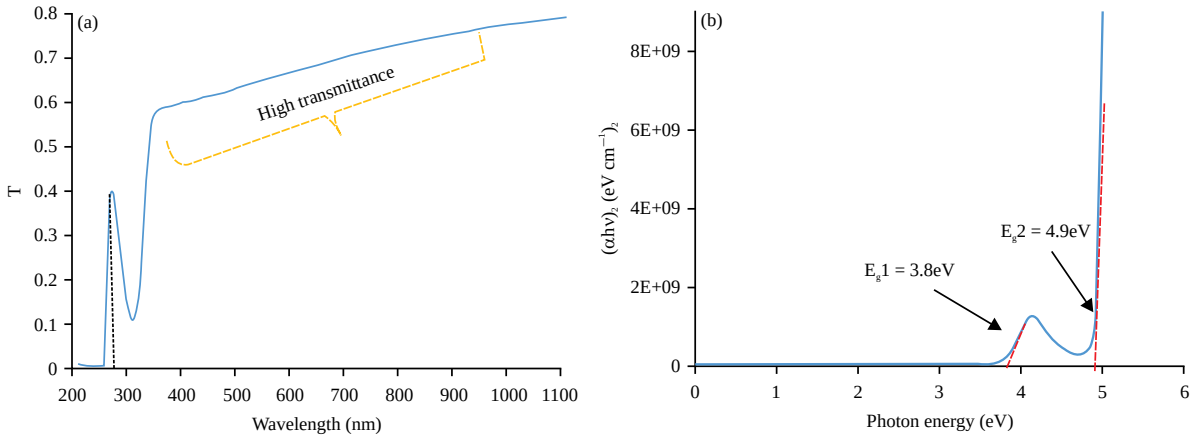

Fig. 5(a-b): (a) Optical transmittance spectra of BaO and (b) Plots of $(\alpha h\nu)_2$ as a function of hν for samples

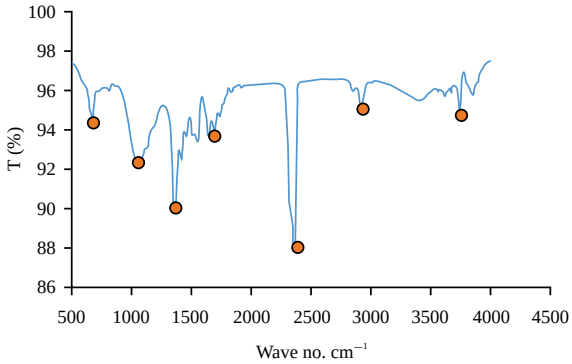

Fig. 6: FTIR of BaO thin film

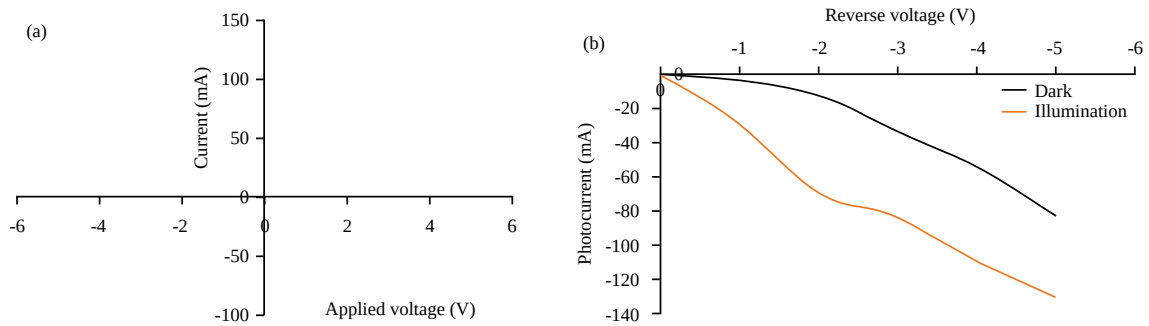

Fig. 7(a-b): I-V characteristics of BaO/PSi/Si heterojuncation under dark and illumination for forward bias and reverse bias

window layer in solar cell applications. It observed the strong peak at 264 nm due to plasmon phenomenon that indicated to formation of nanoparticles in solution. Figure 5b depicts the curve between $(hv)_2$ and photon energy (hv), which provides the direct band gap value. The band gap value is obtained by extrapolating the straight line to the point where $(hv)_2$ = 0. According to the figure, there are two energy gaps caused by high concentrations and the largest of them is 4.35 eV, which is larger than the bulk value because of the quantum size effect[19].

Figure 6 shows the FTIR spectrum for BaO nanoparticles produced using a straightforward chemical process. The presence of the (BaO) stretching vibration mode is indicated by the arrival of the transmission peak at 670 cm^{-1}. While the infrared peaks t (2858.67, 2928.40

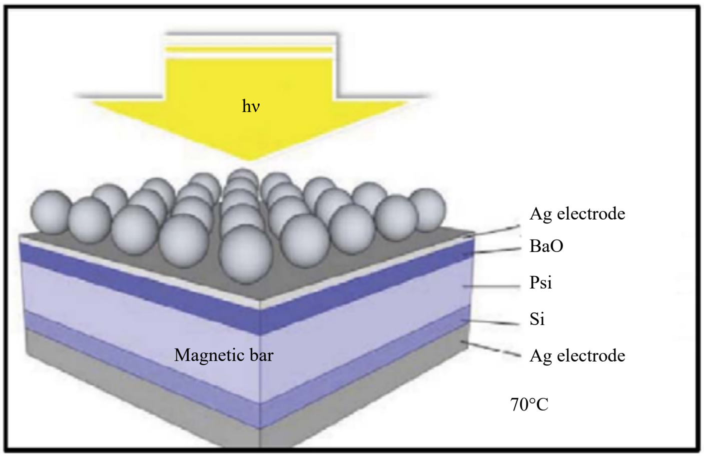

Fig. 8: Schematic diagram represents heterojuncation

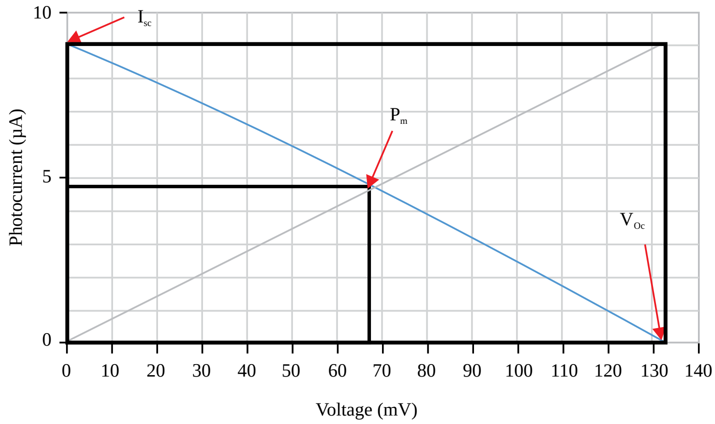

Fig. 9: Isc and Voc curves for Ag/BaO/PSi/Si/Ag heterojuncation solar cell

and 1659 cm^{-1} are the peaks at 3418-3750 and 1363 cm^{-1} correlate to the bonding of (O-H) and harmonics of H-OH stretching bonding modes of water. the bonds C-O at 1075 cm^{-1} and C = C at 2360 cm^{-1}[20].

Figure 7a illustrates the behavior of a PN junction (BaO/PSi/p-Si) under forward and reverse bias in the absence of light at 3 Voltage. Figure 7 shows that the diffusion current is dominant in the forward bias at high voltage, with the forward bias current being larger than the reversal bias current. When illustrated in Fig. 7b, the illumination (100 mW cm^{-2}) for revers bias causes the current to increase as electron-hole production occurs.

Figure 8 depicts the drop casting procedure used to create a heterojunction (Ag/BaO/PSi/Si). They can determine the region on which the heterojunction functions, making the open circuit voltage (Voc) and the short circuit current (Isc) crucial characteristics. The highest power point on the solar power output curve shown in Fig. 9 and the values of Vm (maximum voltage) and Im (maximum current) estimated there. Equation 1 and 2 are used, respectively, to obtain the fill factor and efficiency values. Fill factor and efficiency had values of 27.83 and 0.4%, respectively.

$$F.F = \frac{P_m}{V_{oc} I_{sc}} = \frac{V_m I_m}{V_{oc} I_{sc}}$$

$$Efficiency = \eta = \frac{P_m}{P_{in}} = \frac{F.F\, V_{oc} I_{sc}}{P_{in}} \times 100\%$$

Different loss factors cause the real solar cell's performance to deviate from the ideal instance[21]:

- When the incident photons have energies below the material's band gap (not absorbed and no electron-hole pairs generated). In contrast, incoming photons with energies greater than the material's band gap will be absorbed, producing e-h pairs and dissipating the extra energy as heat
- Light that transmits or reflects without generating e-h couples accounts for around 70% of the energy losses in solar cells

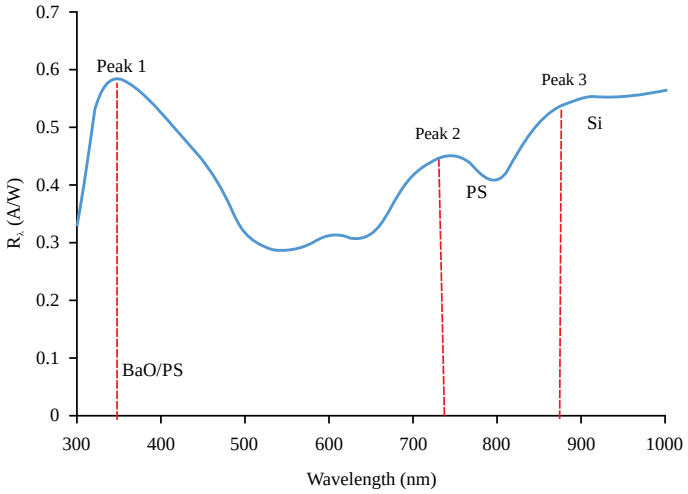

Fig. 10: Shows the responsivity of Ag/BaO/PSi/Si/Ag heterojuncation

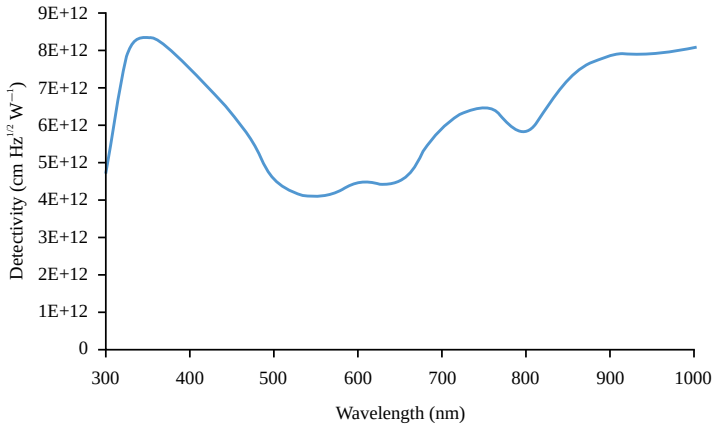

Fig. 11: Shows the detectivity of Ag/BaO/PSi/Si/Ag heterojuncation

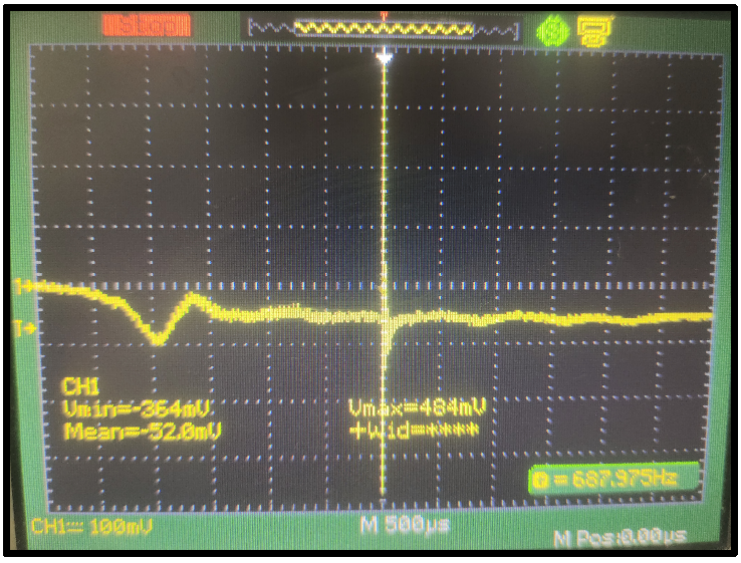

Fig. 12: Lifetime of Ag/BaO/PSi/Si/Ag heterojuncation

- The fill factor may be decreased by each of the recombination processes in depletion zones

The responsiveness of the Ag/BaO/PSi/Si/Ag heterojunction shown in Fig. 10 as a function of wavelength in the range of 300-1100 nm. the first peak at 340 owing to BaO/PSi absorb edge, the second peak at 750 nm due to PSi absorb edge and the third peak at wavelength >750 nm due to Si absorb edge were the three peaks in the responsivity spectrum that were detected. Where the greatest responsivity was measured at 340 nm and was 0.58.

Ag/BaO/PSi/Si/Ag heterojunction detectivity is displayed in Fig. 11 as a function of wavelength in the range of 300-1100 nm, with the detectivity spectra depending on responsiveness as shown in Figure. It noticed that the highest detectivity value ever recorded at 340 nm was 8.2×1012 A/W, which proved the photodetectors suitability for detection. According to Fig. 12, the charge carriers had a free path of 1.4 msec.

CONCLUSION

This research has shown how BaO may be made quickly and cheaply using a straightforward chemical process. The behavior of the sample, as shown by the data, suggests that BaO has positive characteristics and may be employed in a variety of applications, including solar cells and detectors.

REFERENCES

1. Kingsley, U., A.C. Eloka-Eboka and F.L. Inambao, 2017. Review of solar energy inclusion in Africa: Case study of Nigeria. IEA SHC International Conference on Solar Heating and Cooling for Buildings and Industry, https://ukzn-dspace.ukzn.ac.za/bitstream/handle/10413/15357/Ukoba_Kingsley_2017.pdf?sequence=1&isAllowed=y
2. Park, H., D. Kim, J. Jung, D.P. Pham and A.H.T. Le *et al*., 2018. HF etched glass substrates for improved thin-film solar cells. Heliyon, Vol. 4. 10.1016/j.heliyon.2018.e00835.
3. Qin, Y., J. Song, Q. Qiu, Y. Liu, Y. Zhao, L. Zhu and Y. Qiang, 2019. High-quality NiO thin film by low-temperature spray combustion method for perovskite solar cells. J. Alloys Compd., Vol. 810. 10.1016/j.jallcom.2019.151970.
4. Khan, M.I., K.A. Bhatti, R. Qindeel, N. Alonizan and H.S. Althobaiti, 2017. Characterizations of multilayer ZnO thin films deposited by sol-gel spin coating technique. Results Phys., 7: 651-655.
5. Handani, S., Emriadi, D. Dahlan and S. Arief, 2020. Enhanced structural, optical and morphological properties of ZnO thin film using green chemical approach. Vacuum, Vol. 179. 10.1016/j.vacuum.2020.109513.
6. Zaka, H., B. Parditka, Z. Erdélyi, H.E. Atyia, P. Sharma and S.S. Fouad, 2020. Investigation of dispersion parameters, dielectric properties and opto-electrical parameters of ZnO thin film grown by ALD. Optik, Vol. 203. 10.1016/j.ijleo.2019.163933.
7. Ouslimane, T., L. Et-taya, L. Elmaimouni and A. Benami, 2021. Impact of absorber layer thickness, defect density and operating temperature on the performance of $MAPbi_3$ solar cells based on ZnO electron transporting material. Heliyon, Vol. 7. 10.1016/j.heliyon.2021.e06379.
8. Ali, M.Y., M.K.R. Khan, A.M.M.T. Karim, M.M. Rahman and M. Kamruzzaman, 2020. Effect of ni doping on structure, morphology and opto-transport properties of spray pyrolised ZnO nano-fiber. Heliyon, Vol. 6. 10.1016/j.heliyon.2020.e03588.
9. Sundharam, E., A.K.S. Jeevaraj and C. Chinnusamy, 2017. Effect of ultrasonication on the synthesis of barium oxide nanoparticles. J. Bionanoscience, 11: 310-314.
10. Cui, Y., J. Chen, Y. Zhang, X. Zhang, W. Lei, Y. Di and Z. Zhang, 2017. Enhanced performance of thermal-assisted electron field emission based on barium oxide nanowire. Applied Surf. Sci., 396: 1108-1112.
11. Umar, A. and Y.B. Hahn, 2010. Metal oxide nanostructures and their applications. American Scientific Publishers, Stevenson Ranch, https://www.scirp.org/(S(czeh2tfqw2orz553k1w0r45))/reference/referencespapers.aspx?referenceid=788438
12. Renukadevi, R. and S.R. Surfactant, 2019. Surfactant–free, facile synthesis of zinc tungstate nanoparticles for photocatalytic, antibacterial and humidity sensing applications. Int. J. Tech. Inn. Mod. Engg. Sci., 5: 35-42.
13. Renukadevi, R. and R. Sundaram, 2019. Synthesis, characterization, humidity sensing, antibacterial, photocatalytic and kinetic studies of novel $HgWO_4$-WO_3 nanocomposites. Mater. Today: Proc., 8: 153-161.
14. Zhang, Y., Y. Hou, W. Liu, H. Zhang and Y. Zhang *et al*., 2017. A cost-effective relative humidity sensor based on side coupling induction technology. Sensors, Vol. 17. 10.3390/s17050944.
15. Choudhary, V.R., R. Jha and P. Jana, 2006. Epoxidation of styrene by TBHP to styrene oxide using barium oxide as a highly active/selective and reusable solid catalyst. Green Chem., 8: 689-690.

16. Yang, L., Y. Choi, W. Qin, H. Chen and K. Blinn *et al*., 2011. Promotion of water-mediated carbon removal by nanostructured barium oxide/nickel interfaces in solid oxide fuel cells. Nat. Commun., Vol. 2. 10.1038/ncomms1359.
17. Cordoncillo, E., T.R. Machado, L. Ferrazza and D. Juanes, 2012. Synthesis and Characterization of Nanostructured BaO Solutions: Application in Conservation of Wall Paintings. In: Progress in Cultural Heritage Preservation., Ioannides, M., D. Fritsch, J. Leissner, R. Davies, F. Remondino and R. Caffo, (Eds.)., Springer, Berlin, Heidelberg, ISBN-17: 978-3-642-34234-9, pp: 801-808.
18. Ahmad, N., R. Wahab and M. Alam, 2014. Facile growth of barium oxide nanorods: Structural and optical properties. J. Nanosci. Nanotechnol., 14: 5342-5346.
19. Suresh, G. and P.N. Nirmala, 2012. Synthesis of barium oxide nanorod by chemical bath deposition. Turk. J. Phys., 36: 392-397.
20. Naz, F. and K. Saeed, 2022. Synthesis of barium oxide nanoparticles and its novel application as a catalyst for the photodegradation of malachite green dye. Applied Water Sci., Vol. 12. 10.1007/s13201-022-01649-9.
21. vd Laan, C.J. and H.J. Frankena, 1977. Monitoring of optical thin films using a quartz crystal monitor. Vacuum, 27: 391-397.